A Gravity Compensation Strategy for On-ground Validation of Orbital Manipulators

Marco De Stefano[1], Ria Vijayan[1], Andreas Stemmer[1], Ferdinand Elhardt[1] and Christian Ott[2]

***Abstract*— The on-ground validation of orbital manipulators is a challenging task because the robot is designed for a gravity-free operational environment, but it is validated under the effect of gravity. As a consequence, joint torque limits can be easily reached in certain configurations when gravity is actively compensated by the joints. Hence, the workspace for on-ground testing is restricted. In this paper, an optimal strategy is proposed for achieving gravity compensation of an orbital manipulator arm on ground. The strategy minimizes the joint torques acting on the manipulator by solving an optimization problem and it computes the necessary forces to be tracked by an external carrier. Hence, full gravity compensation is achieved for the orbital manipulator. Experimental results validate the effectiveness of the method on the DLR CAESAR space robot, which uses a cable suspended system as external carrier to track the desired gravity compensation force, resulting from the proposed method.**

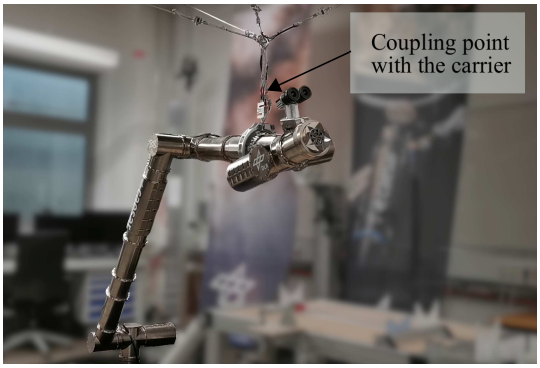

Fig. 1: On-ground validation of a 7 dof orbital manipulator arm (CAESAR in [12]) with an external carrier (cables suspended system) used for gravity compensation.

I. Introduction

Orbital manipulators are a promising technology to perform servicing tasks such as assembly, maintenance, repair, and debris removal in orbit. This was demonstrated in recent mission studies, see e.g. the COMRADE project [1], the e.Deorbit or DEOS mission [2], [3] and the survey on robotic capture in space in [4]. A common characteristic of the manipulators proposed in these mission studies is that they are optimally designed to operate in zero-g (0-g) environment. This factor influences the dimensioning of the joint motors in terms of weight, power and corresponding torque limits. Prior to the launch, an on-ground validation of control algorithms for the orbital manipulator is required. However, the manipulator on ground also experiences the gravitational force, which needs to be actively compensated. A direct compensation at motor level, can negatively affect the workspace of the manipulator during the on-ground testing. In particular, the manipulator can only reach configurations where the torque demanded does not exceed its limits defined for 0-g environment operations.

Several technologies can be adopted to recreate 0-g conditions on ground to validate an orbital manipulator [5], [6]. These can be classified into air bearing, 0-g parabolic flights, neutral buoyancy, hardware-in-the-loop simulator and cable suspended systems. Air bearing systems are floating platforms on a flat floor (see [7], [8], [9]). Pressurised air establishes a thin film between the flat floor and a platform. Hence, the weight of the moving section, e.g. a link of the robotic arm can be compensated. Such a system was used to test the control algorithms of the Japanese free-floating robot [10], the Canadarm and the European Robotic Arm (ERA). However, air bearing systems allow the simulation of 0-g condition only in two dimensional space, which includes one rotation and two translations [11]. In 0-g parabolic flights, an aircraft flying on a parabolic trajectory is exploited to achieve micro-gravity conditions. In [13], experiments were performed in a 0-g parabolic flight for a four degree-of-freedom robot achieving $0.02g$ for only 20 seconds, which duration is not sufficient for a complete validation of complex operations. Another technology for 0-g simulation exploits a water pool to achieve neutral buoyancy, such that the submerged body has a tendency to float as it would be in orbit. The advantage is having six dimensional motion within the fluid and without having time constraints [14], but the drawback is the drag forces induced by the fluid, which generate hydrodynamics effects that distort the dynamics [15]. Hardware-in-the-loop technologies exploit a dynamic model to reproduce a desired behaviour (e.g. floating dynamics) on the hardware. Usually, admittance controlled robot(s) equipped with force-torque sensors are employed [16], [17]. In cable suspended systems, the gravity force is compensated by a system composed of cables, which generate the same force amplitude but in opposite direction of the gravity force vector [18]. This system is currently employed for the on-ground demonstration of assembly tasks in orbit within an ESA project [19]. A controller for modulating the tension in the support cable of a robot to the counterweight is proposed in [20], however, only in a purely vertical direction. A further way to compensate the gravity force acting on a manipulator is to compute it through its dynamics model and actively command it to the joints [21].

[1] The authors are with the Institute of Robotics and Mechatronics, German Aerospace Center (DLR), 82234 Wessling, Germany.

[2] The author is with TU Wien and German Aerospace Center (DLR). Contact: marco.destefano@dlr.de. A video accompanies the paper.

Recently, the CAESAR manipulator arm, was presented as a robotic solution to perform servicing tasks in orbit [12]. The CAESAR arm has 7 degrees-of-freedom (dof) and its design has been optimized for space operation. However, for on-ground validation its workspace is limited by the influence of the gravitational force, that if directly compensated at joints level could exceed its torque limits. To this end, a carrier system (based on cables suspension) is exploited to support the gravity force which CAESAR is subjected to and the set-up is shown in Fig. 1.

Although cable suspended systems already exist in literature, they are usually employed in tasks where only a rigid body is considered (see e.g. [22], [23], [20]). Usually, the tasks of these systems is to position the rigid-body in the workspace and/or to sustain its weight for free-floating dynamics emulation. In contrast to the rigid body case, an orbital manipulator is a multi-body system whose inertia matrix changes as function of its configuration. Hence, also the required gravitational force to be tracked by an external carrier changes and a solution needs to be sought.

The contribution of this paper is twofold. First, a strategy is proposed in order to achieve the gravity compensation and therefore the on-ground validation of an orbital manipulator. The strategy splits the gravity compensation between internal torques of the manipulator and external forces, which can be tracked by an external carrier. To this end, an optimization problem is formulated in order to distribute the gravitational torques between the manipulator and the carrier system. The method is firstly presented for the general case of an orbital arm with an external admittance-controlled carrier. The existence of solution is also presented considering that the carrier could not have a full actuation system to follow all the external force-components. Secondly, for the on-ground validation, a cable suspended system is exploited to track the force resulting from the proposed method. Finally, the gravity compensation of the CAESAR arm is achieved and experimental results are presented.

The paper is structured as follows. Sec. II summarizes the problem statement and Sec. III describes the proposed method. Validation results are presented in Sec. IV with experiment using the CAESAR arm in Sec. IV-B. Sec. V concludes the paper.

II. Problem Statement

A limiting factor for the on-ground validation of space manipulators is that the joint motors are designed for operational requirements in a 0-g environment. Therefore, they cannot support the torque demands in a 1-g environment in the complete workspace. This factor can occur at several robot configurations in the workspace when the configuration-dependent gravitational torques exceed any one of the individual joint torque limits. As a result, the workspace of operation for on-ground testing is limited.

To clearly show the statement of the problem, let us consider the CAESAR arm in a static position as shown in Fig. 2. To actively compensate its weight, the robot has to apply torques and the most loaded joints are J_2 and J_4 with

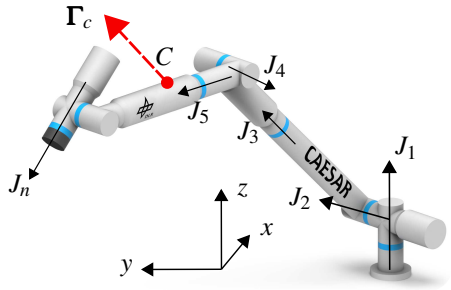

Fig. 2: A 7 dof space manipulator arm. C is the coupling point and Γ_c is the required force/torque wrench which a carrier needs to track. J_n is the rotational axis of the n-joint.

corresponding values $\tau_2 = 369\ Nm$ and $\tau_4 = -135\ Nm$. These values clearly exceed the joint limits of the manipulator ($\pm$ 80 Nm) defined for space operation in [12].

The contribution of the paper is to define a general method which can deliver a desired Cartesian wrench ($\boldsymbol{\Gamma}_c$ in Fig. 2) as input to an external carrier while minimizing the joint torques of the orbital manipulator to respect its torque limits.

III. Proposed Method

In this section, we firstly introduce the modelling of the system and how the gravity forces can be compensated for a generic manipulator-carrier system. To this end, a solution is proposed to provide an optimal distribution of the gravitational torques between the manipulator and the carrier system.

A. Modeling and objective:

Let us introduce the dynamics of a generic manipulator system, as follows,

$$\boldsymbol{H}(\boldsymbol{q})\ddot{\boldsymbol{q}} + \boldsymbol{C}(\boldsymbol{q},\dot{\boldsymbol{q}})\dot{\boldsymbol{q}} + \boldsymbol{G}(\boldsymbol{q}) = \boldsymbol{\tau} + \boldsymbol{J}_c^T(\boldsymbol{q})\boldsymbol{\Gamma}_c \tag{1}$$

where $\boldsymbol{q} \in \mathbb{R}^n$ are joint angle positions for a robot with n joints, and $\dot{\boldsymbol{q}} \in \mathbb{R}^n$ are the joint rates. $\boldsymbol{H}(\boldsymbol{q}) \in \mathbb{R}^{n\times n}$ and $\boldsymbol{C}(\boldsymbol{q},\dot{\boldsymbol{q}}) \in \mathbb{R}^{n\times n}$ are the robot's inertia and Coriolis matrices, and $\boldsymbol{G}(\boldsymbol{q}) \in \mathbb{R}^n$ is the gravitational torque acting on the robot joints. The control torque input to the joints is $\boldsymbol{\tau} \in \mathbb{R}^n$. The external wrench $\boldsymbol{\Gamma}_c \in \mathbb{R}^6$ acting on the system at a contact point C, produces a torque on the joints, transformed with the Jacobian $\boldsymbol{J}_c(\boldsymbol{q}) \in \mathbb{R}^{6\times n}$ at the contact point. The external wrench is composed of $\boldsymbol{\Gamma}_c = \begin{bmatrix}\boldsymbol{F}_c^T & \boldsymbol{T}_c^T\end{bmatrix}^T$ where $\boldsymbol{F}_c \in \mathbb{R}^3$ and $\boldsymbol{T}_c \in \mathbb{R}^3$ are the external force and torque respectively. The control input $\boldsymbol{\tau}$ in (1) can be split into $\boldsymbol{\tau}_g$ for gravity compensation and $\boldsymbol{\tau}_c$ to fulfill the desired control tasks, as:

$$\boldsymbol{\tau} = \boldsymbol{\tau}_g + \boldsymbol{\tau}_c. \tag{2}$$

On-ground robot control methods traditionally employ the gravity-compensation technique to compensate the gravitational torques acting on the joints i.e. by actively applying $\boldsymbol{\tau}_g = \boldsymbol{G}$. Then a suitable feedback-control input $\boldsymbol{\tau}_c$ is designed in joint or Cartesian space (e.g. PD+ control [24], [25]) to achieve the control task. However, the configuration-dependent gravitational torques, can exceed the individual

joint torque limits. This means that active gravity compensation cannot be achieved in these configurations by the manipulator alone. The objective is to distribute the gravitational load acting on the robot, $\boldsymbol{G}$, between the internal joint torques $\boldsymbol{\tau}_g$ and the components of external wrench $\boldsymbol{\Gamma}_c$, which can be applied by an external carrier system. Then, the following relation needs to be satisfied, which does not disturb the control task,

$$\boldsymbol{G} = \boldsymbol{\tau}_g + \boldsymbol{J}_c^T \boldsymbol{\Gamma}_c. \tag{3}$$

$\boldsymbol{\Gamma}_c$ is the external wrench at the contact point (e.g. C in Fig. 2) that a carrier needs to track. Depending on the design of the external carrier and the dofs, it may be possible to apply only certain components of force and/or torque at the contact point. Therefore, let $\boldsymbol{\gamma}_c \in \mathbb{R}^m$ be the independent components of the wrench that can be applied at the contact point C where $1 \leq m \leq 6$. Further, let $\boldsymbol{B}^T \in \mathbb{R}^{6\times m}$ be the wrench basis, that maps $\boldsymbol{\gamma}_c$ to the dimension of the full wrench space. Then the resulting wrench $\boldsymbol{\Gamma}_c$ in (3) is:

$$\boldsymbol{\Gamma}_c = \boldsymbol{B}^T \boldsymbol{\gamma}_c. \tag{4}$$

For example, if the carrier system can only apply a force in the z-direction, then $\boldsymbol{B} = \begin{bmatrix}0 & 0 & 1 & 0 & 0 & 0\end{bmatrix}$ and $\boldsymbol{\gamma_c} \in \mathbb{R}^1$.

Therefore, substituting (4) into (3) we have,

$$\boldsymbol{G} = \boldsymbol{\tau}_g + \boldsymbol{J}_c^T \boldsymbol{B}^T \boldsymbol{\gamma}_c. \tag{5}$$

B. Influence of External Wrench for Gravity Compensation

The contact point C between the robot and the external carrier system can be located at different parts of the manipulator and it determines which of the joint torques the external wrench can influence. Consider that joint numbers $1, 2, .., i$, where $i \leq n$, lie between the fixed-base and contact point of the robot chain. This implies that the Jacobian transformation to the contact point will have the following structure,

$$\boldsymbol{J}_c^T = \begin{bmatrix} \boldsymbol{J}_A^T \\ \boldsymbol{0}_{n-i\times 6} \end{bmatrix} \tag{6}$$

where $\boldsymbol{J}_A \in \mathbb{R}^{6\times i}$ is the Jacobian, which transforms the wrench applied at point C to torques on the joints in the set $A = \{x \mid x \in \mathbb{N},\ x \leq i\}$. The zeros in the lower rows of the Jacobian show that the applied wrench has no influence on the joints in the set $B = \{x \mid x \in \mathbb{N}, i < x \leq n\}$. This is because the joints in set B are between the contact point and the free end-effector in the robot chain. This implies that we can further simplify (5) using (6) and split the terms between joints in set A and B as,

$$\boldsymbol{G} = \begin{bmatrix} \boldsymbol{G}_A \\ \boldsymbol{G}_B \end{bmatrix} = \begin{bmatrix} \boldsymbol{\tau}_{gA} \\ \boldsymbol{\tau}_{gB} \end{bmatrix} + \begin{bmatrix} \boldsymbol{J}_A^T \boldsymbol{B}^T \boldsymbol{\gamma}_c \\ \boldsymbol{0}_{n-i\times 1} \end{bmatrix} \tag{7}$$

where $\boldsymbol{G}_A$ and $\boldsymbol{G}_B$ are the gravitational torques of the joints in set A and B. Similarly, $\boldsymbol{\tau}_{gA}$ and $\boldsymbol{\tau}_{gB}$ are the manipulator gravity compensating torques for the joints in the set A and B. As we see from (7), the external wrench applied cannot influence joints in the set B, therefore these joints shall be commanded with the gravitational torques computed from the dynamics model as they are, i.e $\boldsymbol{\tau}_{gB} = \boldsymbol{G}_B$. Then from a practical perspective, the location of C should be chosen such that $\boldsymbol{G}_B$ does not exceed the torque limits for the workspace of interest. This needs to be taken into account in the design stage considering that the joints closer to the free end-effector of the robot anyway experience less gravitational torques.

The remaining joint torques $\boldsymbol{\tau}_{gA}$ and the external wrench components $\boldsymbol{\gamma_c}$ can be designed to distribute the gravitational load between the two quantities while satisfying some optimality criteria such that the following relation from (7) holds,

$$\boldsymbol{G}_A = \boldsymbol{\tau}_{gA} + \boldsymbol{J}_{cA}^T \boldsymbol{\gamma}_c \tag{8}$$

where the contact Jacobian $\boldsymbol{J}_{cA}^T = \boldsymbol{J}_A^T \boldsymbol{B}^T$. Note that in general $\boldsymbol{J}_{cA}^T$ is not square and therefore not invertible. Hence we cannot solve for $\boldsymbol{\gamma}_c$ directly by, for example, setting the torques $\boldsymbol{\tau}_{gA} = \boldsymbol{0}$. Hence, an optimal solution is sought for the distribution of external forces and joint motor torques.

C. Optimal Solution

In order to optimally distribute the gravity-compensation torques between the joint motors and the external carrier, we define the following optimization problem using (8) as a constraint,

$$\min_{(\boldsymbol{\tau}_{gA}, \boldsymbol{\gamma_c})} \quad \frac{1}{2} \begin{bmatrix} \boldsymbol{\tau}_{gA}^T & \boldsymbol{\gamma}_c^T \end{bmatrix} \begin{bmatrix} \boldsymbol{W}_\tau & \boldsymbol{0} \\ \boldsymbol{0} & \boldsymbol{W}_\gamma \end{bmatrix} \begin{bmatrix} \boldsymbol{\tau}_{gA} \\ \boldsymbol{\gamma_c} \end{bmatrix} \tag{9}$$

$$\text{s.t. } \boldsymbol{G}_A = \boldsymbol{\tau}_{gA} + \boldsymbol{J}_{cA}^T \boldsymbol{\gamma}_c \tag{10}$$

where $\boldsymbol{W}_\tau \in \mathbb{R}^{i\times i}$ and $\boldsymbol{W}_\gamma \in \mathbb{R}^{m\times m}$ are the weighting matrices for the joint torques and external wrench components. Note here that the input from the robot $\boldsymbol{\tau}_{gA}$, and the input from the carrier system $\boldsymbol{\gamma}_c$, are not coupled in the cost function in (9), since the inputs come from two separate hardware systems.

To solve the optimization problem, the Lagrange multiplier methods is considered and the objective function is augmented by the constraint equations through a set of non-negative multiplicative Lagrange multipliers, $\boldsymbol{\lambda} \geq 0$ as,

$$L = \frac{1}{2} \begin{bmatrix} \boldsymbol{\tau}_{gA}^T & \boldsymbol{\gamma_c}^T \end{bmatrix} \begin{bmatrix} \boldsymbol{W}_\tau & \boldsymbol{0} \\ \boldsymbol{0} & \boldsymbol{W}_\gamma \end{bmatrix} \begin{bmatrix} \boldsymbol{\tau}_{gA} \\ \boldsymbol{\gamma}_c \end{bmatrix} + \boldsymbol{\lambda}^{\boldsymbol{T}} (\boldsymbol{G}_A - \boldsymbol{\tau}_{gA} - \boldsymbol{J}_{cA}^T \boldsymbol{\gamma}_c). \tag{11}$$

The minimum of the modified function L satisfying the constraint, is computed as

$$\nabla L(\boldsymbol{x}, \boldsymbol{\lambda}) = 0, \quad \text{with } \boldsymbol{x} = (\boldsymbol{\tau}_{gA}, \boldsymbol{\gamma}_c) \tag{12}$$

which leads to,

$$\frac{\partial L}{\partial \boldsymbol{\tau}_{gA}} = \boldsymbol{W}_\tau \boldsymbol{\tau}_{gA} - \boldsymbol{\lambda} = 0 \tag{13}$$

$$\frac{\partial L}{\partial \boldsymbol{\gamma}_c} = \boldsymbol{W}_\gamma \boldsymbol{\gamma}_c - \boldsymbol{J}_{cA} \boldsymbol{\lambda} = 0 \tag{14}$$

$$\frac{\partial L}{\partial \boldsymbol{\lambda}} = \boldsymbol{G}_A - \boldsymbol{\tau}_{gA} - \boldsymbol{J}_{cA}^T \boldsymbol{\gamma}_c = 0 \tag{15}$$

From (13) and (15), the Lagrangian multiplier results as

$$\boldsymbol{\lambda} = \boldsymbol{W}_\tau (\boldsymbol{G}_A - \boldsymbol{J}_{cA}^T \boldsymbol{\gamma}_c) \tag{16}$$

and substituting (16) in (14), the optimal wrench components, $\boldsymbol{\gamma}_c^*$, result in

$$\boldsymbol{\gamma}_c^* = (\boldsymbol{W}_\gamma + \boldsymbol{J}_{cA} \boldsymbol{W}_\tau \boldsymbol{J}_{cA}^{\boldsymbol{T}})^{-1} \boldsymbol{J}_{cA} \boldsymbol{W}_\tau \boldsymbol{G}_A. \tag{17}$$

TABLE I

Case	Weight	Dimensionality			Singularity-independent
		$i > m$	$i = m$	$i < m$	
(i)	$\boldsymbol{W}_\tau > 0$, $\boldsymbol{W}_\gamma = 0$	$\boldsymbol{\gamma}_c^* = (\boldsymbol{J}_{cA}\boldsymbol{W}_\tau\boldsymbol{J}_{cA}^{\boldsymbol{T}})^{-1}\boldsymbol{J}_{cA}\boldsymbol{W}_\tau\boldsymbol{G}_A$ $\boldsymbol{\tau}_{gA}^* = \left(\boldsymbol{I} - \boldsymbol{J}_{cA}^{\boldsymbol{T}}(\boldsymbol{J}_{cA}\boldsymbol{W}_\tau\boldsymbol{J}_{cA}^{\boldsymbol{T}})^{-1}\boldsymbol{J}_{cA}\boldsymbol{W}_\tau\right)\boldsymbol{G}_A$	$\boldsymbol{\gamma}_c^* = \boldsymbol{J}_{cA}^{-T}\boldsymbol{G}_A$ and $\boldsymbol{\tau}_{gA}^* = \boldsymbol{0}$	ill-posed	✗
(ii)	$\boldsymbol{W}_\tau = 0$, $\boldsymbol{W}_\gamma > 0$	$\boldsymbol{\gamma}_c^* = \boldsymbol{0}$ and $\boldsymbol{\tau}_{gA}^* = \boldsymbol{G_A}$			✓
(iii)	$\boldsymbol{W}_\tau > 0$, $\boldsymbol{W}_\gamma > 0$	$\boldsymbol{\gamma}_c^*$ as in (17) and $\boldsymbol{\tau}_{gA}^*$ as in (18)			✓

Optimal solutions of problem in (9) and (10) summarized for various cases of weighting matrices, dimensionality and singularity. *i*: dimension of the gravity-compensated joints, *m*: dimension of the external wrench components (carrier).

The optimized joint torques, $\boldsymbol{\tau}_{gA}^*$, can be obtained by substituting (17) in (10), which results as follows,

$$\boldsymbol{\tau}_{gA}^* = \left(\boldsymbol{I} - \boldsymbol{J}_{cA}^{\boldsymbol{T}}(\boldsymbol{W}_\gamma + \boldsymbol{J}_{cA}\boldsymbol{W}_\tau\boldsymbol{J}_{cA}^{\boldsymbol{T}})^{-1}\boldsymbol{J}_{cA}\boldsymbol{W}_\tau\right)\boldsymbol{G}_A. \qquad (18)$$

The solutions in (17) and (18) optimally distribute the gravitational torques $\boldsymbol{G}_A$ between $\boldsymbol{\gamma}_c$ and $\boldsymbol{\tau}_{gA}$. In particular, (17) is the desired force to be tracked by the external carrier and (18) is the joint torque input to the manipulator for the joints in the set A. The existence of solutions (17)-(18) is summarized in Table I and discussed as follows, where $\boldsymbol{A} > \boldsymbol{0}$ denotes that the generic matrix $\boldsymbol{A}$ is positive definite.

Case (i): $\boldsymbol{W}_\tau > \boldsymbol{0}$ and $\boldsymbol{W}_\gamma = \boldsymbol{0}$. The existence of the solution depends on the dimensionality of the external wrench of the robot-carrier and the rank of the Jacobian:

- When $i > m$ the dimension of the joints i, that can be gravity-compensated, is greater than the dimension of the external wrench components m. The solution exists only in singularity-free robot configurations. In this case, the joint torques resulting from the optimized external wrench components, $\boldsymbol{J}_{cA}^T\boldsymbol{\gamma}_{\boldsymbol{c}}^*$, projects $\boldsymbol{G}_A$ onto the range space (image) of $\boldsymbol{J}_{cA}^T$, and $\boldsymbol{\tau}_{gA}^*$ in (18) projects $\boldsymbol{G}_A$ onto the nullspace (kernel) of $\boldsymbol{J}_{cA}^T$. In other words, the joint torques that cannot be generated by the external wrench carrier are actively compensated by the manipulator joint torques.
- When $i = m$ the dimension of the joints i is equal to the dimension of the external wrench components m. In this case, $\boldsymbol{J}_{cA}^T$ is square and in singularity-free robot configurations, $\boldsymbol{\gamma}_c^*$ is obtained using the inverse of the transposed-Jacobian. In other words, the carrier system can fully compensate the gravity torques and no joint torques need to be applied.
- When $i < m$ the dimension of the joints i, that can be gravity-compensated, is less than the dimension of the external wrench components m. In this case, setting $\boldsymbol{W}_\gamma = \boldsymbol{0}$ makes the problem ill-posed. This does not represent a limitation in the physical capability of the carrier system, but only in the problem definition because there is no metric with respect to which an optimal solution is to be solved. Note that the least cost in (9) would be obtained for $\boldsymbol{\tau}_{gA}^* = \boldsymbol{0}$. In this case, being $\boldsymbol{J}_{cA}^T$ a $i \times m$ matrix, with $i < m$, the problem is still under-constrained, as seen from (10). This leads having several solutions for $\boldsymbol{\gamma}_c$, but since $\boldsymbol{W}_\gamma = \boldsymbol{0}$, none of the solutions can be chosen, hence, the problem is ill-posed. Then, to have an optimal solution when $i < m$ it is convenient to set the weight $\boldsymbol{W}_\gamma$ to a non-zero value.

Case (ii)[1]*:* When $\boldsymbol{W}_\tau = \boldsymbol{0}$ and $\boldsymbol{W}_\gamma > \boldsymbol{0}$, there is no limitation on internal joint motor torques, then $\boldsymbol{\gamma}_c^* = \boldsymbol{0}$, $\boldsymbol{\tau}_{gA}^* = \boldsymbol{G}_A$ and the solution is singularity-independent.

Case (iii): When $\boldsymbol{W}_\tau > \boldsymbol{0}$ and $\boldsymbol{W}_\gamma > \boldsymbol{0}$, an optimal solution always exists. This is independent of the rank of the Jacobian or the dimensionality of the external wrench components, since the invertibility of the weighted terms in (17) and (18) is determined by the positive-definiteness of $\boldsymbol{W}_\gamma$. Therefore, a solution exists even for singular-configurations of the robot.

The proposed strategy is summarized with a schematic in Fig. 3. From the measured joint positions, $\boldsymbol{q}$, the dynamics and kinematics (*Dyn./Kinem.*) of the manipulator arm is computed. The corresponding Jacobian at the coupling point, $\boldsymbol{J}_c$ and the vector $\boldsymbol{G}_A$ are the input to the optimizer, whose outputs are sent to the external carrier and the orbital manipulator. Note that the final gravity torque input for the manipulator is $\boldsymbol{\tau}_g^* = [\boldsymbol{\tau}_{gA}^*; \boldsymbol{\tau}_{gB}]$. This includes the optimized torque, $\boldsymbol{\tau}_{gA}^*$ and the gravity torque for the joints in set *B* (between the contact point and the free end-effector of the robot chain). From Fig. 3, it can be seen that the proposed strategy will not interfere with the validation of a controller, i.e. the independent torque input $\boldsymbol{\tau}_c$.

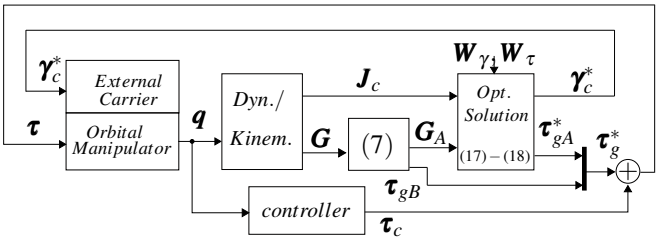

Fig. 3: Schematic of the proposed method to achieve gravity compensation on-ground.

Note that from a practical perspective, the external carrier could have hardware limits in applying, e.g., a minimum force $\boldsymbol{\gamma}_c$. This could be taken into account in the solution while adding additional inequality constrains for the optimization problem in (9), (10). In this case, numerical solvers could be also employed, see e.g. qpOASES in [26], which is used also for robotic implementation in real-time [27].

[1]This case is reported for completeness, but it assumes that the manipulator can already apply sufficient torques on ground to sustain its weight.

IV. Validation and Experimental Results

In this section we show simulation and experimental results obtained with the proposed method. The considered orbital manipulator is the CAESAR arm, which is a torque controlled robot composed of 7 dof with a length of about 2.4 m in stretched configuration. Its weight is about 60 kg and the maximum joint torque allowable is $\pm$ 80 Nm, see [12]. The weighting matrices are defined as $\boldsymbol{W}_\tau = diag(1/\tau_{i,max}^2)$ where $\tau_{i,max}$ is the maximum torque of the i-th joint and $\boldsymbol{W}_\gamma = diag(1/\gamma_{i,max}^2)$, where $\gamma_{i,max}$, is the maximum of the external component of wrench. To show the flexibility of the method, the validation in simulation and experiment considers different points C of application of the force and different carriers, which can track different components of the external wrench.

A. Simulation Results

To show the flexibility of the method, let us assume that the contact point C is located e.g. at J_4 (see Fig. 2) and the external carrier can provide tracking of force in x-y-z and torque only in x and y. This means that the set A, which lies between the fixed-base and contact point C, is $A = \{1,2,3,4\}$, $B = \{5,6,7\}$ and the wrench basis of the carrier will be $\boldsymbol{B} = [\boldsymbol{I}_{5\times5}\ \boldsymbol{0}_{5\times1}]$. The weight $\tau_{i,max} = 80\ Nm$ is chosen for $\boldsymbol{W}_\tau$ and $\gamma_{i,max} = 500\ N,Nm$ is chosen for $\boldsymbol{W}_\gamma$.

From the initial configuration shown in Fig. 2 a relative position in Cartesian frame of $[-0.3\ 0.1\ -0.15]$ m and a relative orientation of $[40\ 5\ 12]$ deg is commanded to the tool of the CAESAR arm using an impedance Cartesian controller (PD+, see [28, eq. (7)]). The position and orientation error of the controller during the motion is shown in Fig. 4.

The benefit of the proposed method is shown in Fig. 5. If the proposed method is not applied, the gravitational torques required by the arm will exceed the limit of $\pm$ 80Nm (see Fig. 5 (left) with values reaching 370 Nm and -130 Nm).

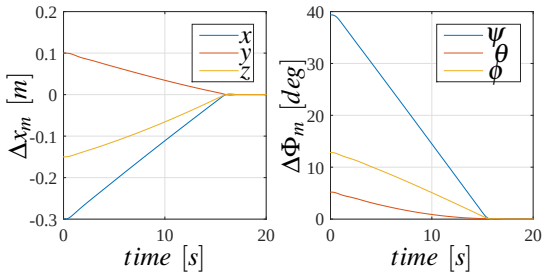

Fig. 4: Error in position and orientation during the motion.

Fig. 5 (right) shows the gravity torque in the set A resulting from the proposed method. As can be seen, the maximum torque now is less than 3 Nm. To fully achieve compensation of the gravity force, the carrier needs to track a required wrench, which is the output of the proposed method and this can be found in Fig. 6 (left). For validation purposes, Fig. 6 (right) shows the same force, but transformed in the joint space of the manipulator. From Fig. 5 and Fig. 6 (right), it can be see that full gravity compensation of $\boldsymbol{G}_A$ is achieved and the constraint in (10) is satisfied.

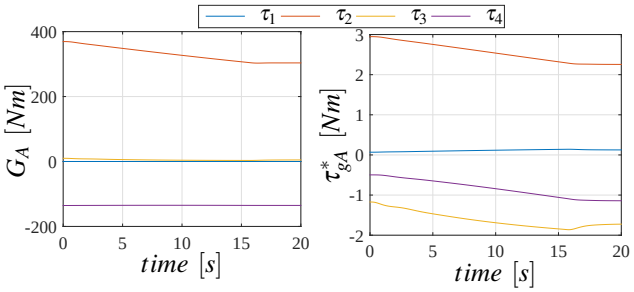

Fig. 5: Left: gravity torques required by the arm without the proposed strategy. Right: torques with the proposed method.

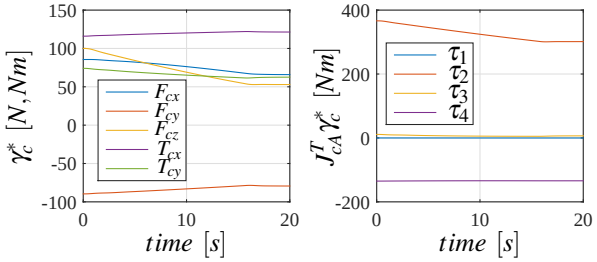

Fig. 6: Left: wrench for the carrier resulting from the optimal solution. Right: corresponding wrench transformed in the joint space of manipulator.

B. Experiments with the CAESAR Robot-Carrier system

A cable-driven system is used as external carrier [29] and it is connected to the CAESAR arm through a coupling mechanism at the point C, as shown in Fig. 7. The control of the carrier runs at 4 kHz and it is able to follow a desired Cartesian force using an admittance control [30]. As such, the desired force is the input to a dynamic model where acceleration is computed and discretely integrated. Thus, a new set-point is provided to the cable-driven system through the inverse kinematic [31], [32]. The considered carrier in Fig. 7 has four motors and it can apply and track only translational forces along the components $x-y-z$ at the contact point C, but no torques. This implies that the wrench basis is, $\boldsymbol{B} = [\boldsymbol{I}_{3\times3}\ \boldsymbol{0}_{3\times3}]$. Further, the location of the coupling

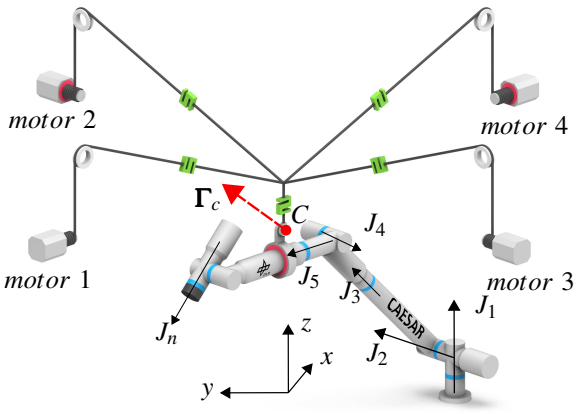

Fig. 7: A 7 dof space manipulator coupled with a cable suspended unit as carrier. C is the coupling point between the systems.

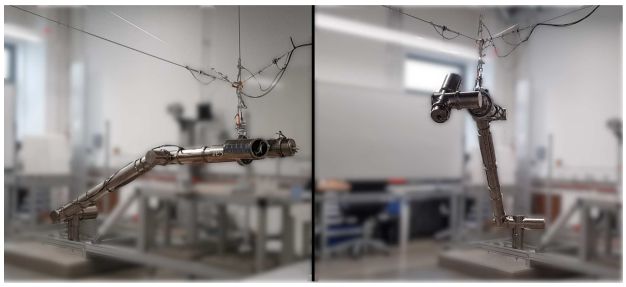

Fig. 8: Motion of CAESAR with the external carrier during the experiment between its initial pose (left) to the final one (right).

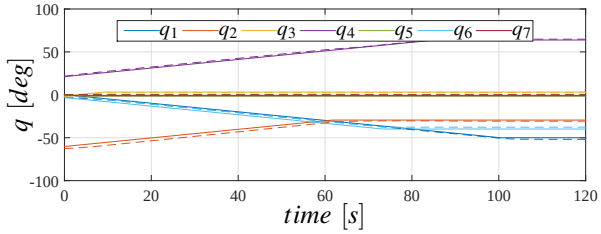

Fig. 9: Joint position during the experiment: commanded (dashed line) and measured (solid line).

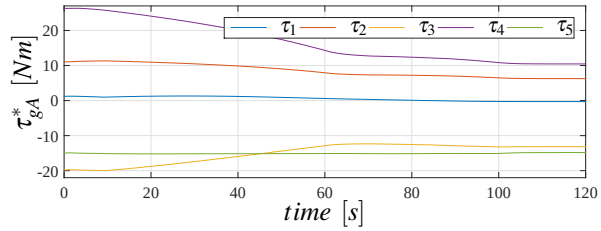

Fig. 10: Optimal joint torques applied to CAESAR.

point C was chosen after J_5 such that $\boldsymbol{G}_B$ does not exceed the torque limits for the expected workspace of interest. Hence, the set A results in $A = \{1,2,3,4,5\}$ and the set between the contact point and the free end-effector $B = \{6,7\}$. As explained in Sec. III with (7), $\boldsymbol{\tau}_{gB} = \boldsymbol{G}_B$, i.e. the force applied at point C cannot influence the joint in set B. The weights are chosen as $\tau_{i,max} = 80\ Nm$ and $\gamma_{i,max} = 750\ N$.

The experiment considers the motion of CAESAR from its initial pose shown in Fig. 8 (left) to a final one (right) using a joint impedance controller [21] at 1 kHz. The joints position trajectory commanded to the robot is shown in Fig. 9 and compared with the measured data. The optimal gravitational torques given by the proposed method are shown in Fig. 10 and commanded to the CAESAR arm. As it can be seen, they are below the considered torque limits of 80 Nm. The optimal forces generated for the carrier are shown in Fig. 11 and compared with the measured values by the carrier system. The error in force tracking $\Delta\boldsymbol{\gamma}^*_c$ is below 4 N and approaches close to zero in static pose (see after 100s). For validation purposes, the required gravity torque during the motion, $\boldsymbol{G}_A$, is compared with the total forces (internal joint torques and external forces of the carrier) acting on the manipulator. This is computed from the measurement as, $\bar{\boldsymbol{\tau}}_A = \boldsymbol{\tau}_{msr,A} - \boldsymbol{\tau}_{c,A} + \boldsymbol{J}^T_{CA}\boldsymbol{\gamma}^*_{c_{msr}}$, where (msr,A) indicates the corresponding measured value in the set A. The comparison

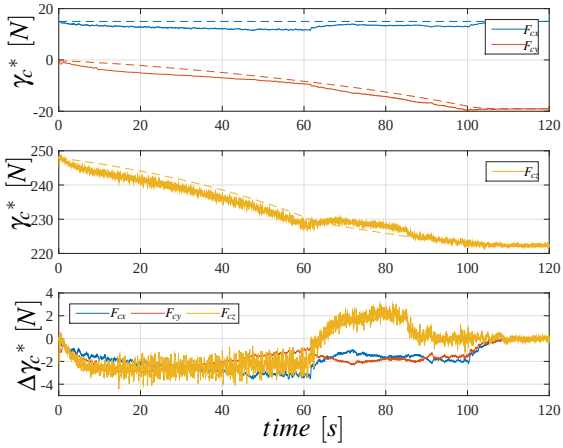

Fig. 11: Optimal force of the external carrier in x-y (Top), z (middle). Bottom: Error between commanded (dashed line) and measured (solid line) force of the carrier.

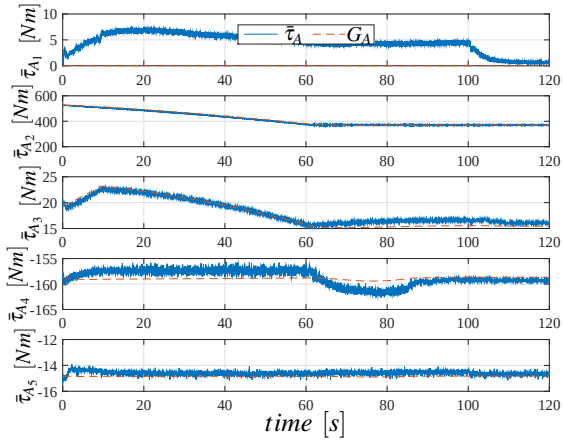

Fig. 12: Comparison between the required gravity torque $\boldsymbol{G}_A$ and the overall gravity torque acting on the manipulator joint space, $\bar{\boldsymbol{\tau}}_A$, (computed from the measured data).

is shown in Fig. 12, where the major error is recorded on joint 1, which is caused by the admittance-controlled carrier during tracking. However, in static pose the error goes to zero (see after 100s). This experiment shows that the proposed strategy is suitable for the on-ground testing of orbital manipulator. Further experiments can be seen in the video accompanying the paper.

V. Conclusion and Future Works

In this paper, a strategy has been proposed in order to compensate the gravity of a space manipulator for on-ground testing. The approach resolves an optimal problem, which minimizes the joints torque and provides as output a desired force to be tracked by an external carrier. Experimental results with the CAESAR arm show the effectiveness of the method where a cable suspended system was used as a carrier to track the desired compensation force. The proposed method is general enough that it can be applied also to any other manipulator with different coupling point or external carriers, e.g. industrial robot. Future works aim at increasing the robustness under noise and dynamics uncertainties.

REFERENCES

[1] P. Colmenarejo, N. Santos, P. Serra, J. Telaar, H. Strauch, M. De Stefano, A. M. Giordano, H. Mishra, R. Lampariello, C. Ott, *et al.*, "Results of the comrade project: combined control for robotic spacecraft and manipulator in servicing missions: active debris removal and re-fuelling," in *11th International ESA Conference on Guidance, Navigation & Control Systems*, 2020.

[2] D. Henry, J. Cieslak, J. Z. Torres, P. Colmenarejo, J. Branco, N. Santos, P. Serra, J. Telaard, H. Strauch, A. Giordano, M. De Stefano, C. Ott, M. Reiner, J. Jaworsk, E. Papadopoulos, G. Visentin, F. Ankersen, and J. Fernandez, "Model-based fault diagnosis and tolerant control: the esa's e.deorbit mission," in *2019 18th European Control Conference (ECC)*, 2019, pp. 4356–4361.

[3] P. Rank, Q. Mühlbauer, W. Naumann, and K. Landzettel, "The deos automation and robotics payload," in *Symp. on Advanced Space Technologies in Robotics and Automation, ASTRA, the Netherlands*, 2011.

[4] E. Papadopoulos, F. Aghili, O. Ma, and R. Lampariello, "Robotic manipulation and capture in space: A survey," *Frontiers in Robotics and AI*, vol. 8, 2021.

[5] J. L. Schwartz, M. A. Peck, and C. D. Hall, "Historical review of air-bearing spacecraft simulators," in *Journal of Guidance, Control and Dynamics*, 2003, pp. AAS 03–125.

[6] Y. R. Chheta, R. M. Joshi, K. K. Gotewal, and M. ManoahStephen, "A review on passive gravity compensation," in *2017 International conference of Electronics, Communication and Aerospace Technology (ICECA)*, vol. 1, 2017, pp. 184–189.

[7] Y. Umetani and K. Yoshida, "Experimental study on two-dimensional free-flying robot satellite model," in *JPL, California Inst. of Tech., Proceedings of the NASA Conference on Space Telerobotics, Volume 5*, 1989.

[8] M. Marchesi, F. Angrilli, and C. Bettanini, "On ground experiments of free-flyer space robot simulator in intervention missions," in *proceedings of 6th International Symposium on Artificial Intelligence, Robotics and Automation in Space i-SAIRAS*, 2001.

[9] K. Yoshida, "Experimental study on the dynamics and control of a space robot with experimental free-floating robot satellite," *Advanced Robotics*, vol. 9, no. 6, p. 583602, 1994. [Online]. Available: https://doi.org/10.1163/156855395X00319

[10] ——, "Engineering test satellite vii flight experiments for space robot dynamics and control: Theories on laboratory test beds ten years ago, now in orbit," *The International Journal of Robotics Research*, vol. 22, no. 5, pp. 321–335, 2003.

[11] C. Menon, S. Busolo, S. Cocuzza, A. Aboudan, A. Bulgarelli, C. Bettanini, M. Marchesi, and F. Angrilli, "Issues and solutions for testing free-flying robots," *Acta Astronautica*, vol. 60, no. 12, pp. 957 – 965, 2007.

[12] A. Beyer, G. Grunwald, M. Heumos, M. Schedl, R. Bayer, W. Bertleff, B. Brunner, R. Burger, J. Butterfaß, R. Gruber, *et al.*, "Caesar: Space robotics technology for assembly, maintenance, and repair," in *Proceedings of the International Astronautical Congress, IAC*, 2018.

[13] H. Sawada, K. Ui, M. Mori, H. Yamamoto, R. Hayashi, S. Matunaga, and Y. Ohkami, "Micro-gravity experiment of a space robotic arm using parabolic flight," *Advanced Robotics*, vol. 18, no. 3, pp. 247–267, 2004.

[14] C. R. Carignan and D. L. Akin, "The reaction stabilization of on-orbit robots," *IEEE Control Systems Magazine*, vol. 20, no. 6, pp. 19–33, Dec 2000.

[15] A. Flores-Abad, O. Ma, K. Pham, and S. Ulrich, "A review of space robotics technologies for on-orbit servicing," *Progress in Aerospace Sciences*, vol. 68, pp. 1 – 26, 2014.

[16] M. De Stefano, H. Mishra, A. M. Giordano, R. Lampariello, and C. Ott, "A relative dynamics formulation for hardware- in-the-loop simulation of on-orbit robotic missions," *IEEE Robotics and Automation Letters*, vol. 6, no. 2, pp. 3569–3576, 2021.

[17] N. Muraleedharan, D. R. Isenberg, and I. Gentilini, "Recreating planar free-floating environment via model-free force-feedback control," in *2016 IEEE Aerospace Conference*, 2016, pp. 1–12.

[18] H. B. Brown and J. M. Dolan, "A Novel Gravity Compensation System for Space Robots," in *Robotics Institute. Paper 217*, 1 1994.

[19] M. Deremetz *et al.*, "Demonstrator design of a modular multi-arm robot for on-orbit large telescope assembly," in *Advanced Space Technologies for Robotics and Automation (ASTRA)*, 2022.

[20] G. C. White and Y. Xu, "An active vertical-direction gravity compensation system," *IEEE transactions on instrumentation and measurement*, vol. 43, no. 6, pp. 786–792, 1994.

[21] B. Siciliano, L. Sciavicco, L. Villani, and G. Oriolo, *Robotics: Modelling, Planning and Control - Chapter 8: Motion Control*, 1st ed. Springer Publishing Company, Incorporated, 2008.

[22] R. Boumann, P. Lemmen, R. Heidel, and T. Bruckmann, "Optimization of trajectories for cable robots on automated construction sites," in *Proceedings of the 37th International Symposium on Automation and Robotics in Construction (ISARC)*, October 2020, pp. 465–472.

[23] A. Pott, H. Mtherich, W. Kraus, V. Schmidt, P. Miermeister, T. Dietz, and A. Verl, "Cable-driven parallel robots for industrial applications: The ipanema system family," in *IEEE ISR 2013*, 2013, pp. 1–6.

[24] B. Paden and R. Panja, "Globally asymptotically stable pd+ controller for robot manipulators," *International Journal of Control*, vol. 47, no. 6, pp. 1697–1712, 1988.

[25] A. Albu-Schäffer, C. Ott, and G. Hirzinger, "A unified passivity-based control framework for position, torque and impedance control of flexible joint robots," *The international journal of robotics research*, vol. 26, no. 1, pp. 23–39, 2007.

[26] H. J. Ferreau, C. Kirches, A. Potschka, H. G. Bock, and M. Diehl, "qpoases: A parametric active-set algorithm for quadratic programming," *Mathematical Programming Computation*, vol. 6, no. 4, pp. 327–363, 2014.

[27] B. Henze, M. A. Roa, and C. Ott, "Passivity-based whole-body balancing for torque-controlled humanoid robots in multi-contact scenarios," *The International Journal of Robotics Research*, vol. 35, no. 12, pp. 1522–1543, 2016.

[28] M. De Stefano, H. Mishra, R. Balachandran, R. Lampariello, C. Ott, and C. Secchi, "Multi-rate tracking control for a space robot on a controlled satellite: A passivity-based strategy," *IEEE Robotics and Automation Letters*, vol. 4, no. 2, pp. 1319–1326, 2019.

[29] F. Elhardt *et al.*, "The motion suspension system-MSS: A cable-driven system for on-ground tests of space robots," in *16th IFToMM World Congress, Tokyo, Japan (submitted)*, 2023.

[30] W. Yang Ho, W. Kraus, A. Mangold, and A. Pott, "Haptic interaction with a cable-driven parallel robot using admittance control," in *Cable-Driven Parallel Robots*, A. Pott and T. Bruckmann, Eds. Cham: Springer International Publishing, 2015, pp. 201–212.

[31] M. De Stefano, R. Balachandran, J. Artigas, and C. Secchi, "Reproducing physical dynamics with hardware-in-the-loop simulators: A passive and explicit discrete integrator," in *Robotics and Automation (ICRA), 2017 IEEE International Conference on*, May 2017, pp. 5899–5906.

[32] A. A. Kumar, J.-F. Antoine, and G. Abba, "Control of an underactuated 4 cable-driven parallel robot using modified input-output feedback linearization," *IFAC-PapersOnLine*, vol. 53, no. 2, pp. 8777–8782, 2020.